A Mechanism for Explaining the Maximum Intraseasonal Oscillation Center over the Western North Pacific*

FEI LIU AND BIN WANG

International Pacific Research Center, and Department of Meteorology, University of Hawai'i at Mānoa, Honolulu, Hawaii

(Manuscript received 13 November 2012, in final form 24 September 2013)

ABSTRACT

During late boreal summer (July–October), the intraseasonal oscillation (ISO) exhibits maximum variability over the western North Pacific (WNP) centered in the South China Sea and Philippine Sea, but many numerical models have difficulty in simulating this essential feature of the ISO. To understand why this maximum variability center exists, the authors advance a simple box model to elaborate the potential contribution of the mean-state-dependent atmosphere–ocean interaction. The model results suggest that the WNP seasonal mean monsoon trough plays an essential role in sustaining a strong stationary ISO, contributing to the existence of the maximum intraseasonal variability center. First, the monsoon trough provides abundant moisture supply for the growing ISO disturbances through the frictional boundary layer moisture convergence. Second, the cyclonic winds associated with the monsoon trough provide a favorable basic state to support a negative atmosphere–ocean thermodynamic feedback that sustains a prominent stationary ISO. In an active phase of the ISO, anomalous cyclonic winds enhance the monsoon trough and precipitation, which reduce shortwave radiation flux and increase evaporation; both processes cool the sea surface and lead to an ensuing high pressure anomaly and a break phase of the ISO. In the wintertime, however, the wind–evaporation feedback is positive and sustains the Philippine Sea anticyclone. The result here suggests that accurate simulation of the boreal summer climatological mean state is critical for capturing a realistic ISO over the WNP region.

1. Introduction

The tropical intraseasonal oscillation (ISO) with a period of 30–60-day experiences pronounced seasonality (Madden 1986; Wang and Rui 1990a; Kemball-Cook and Wang 2001). During boreal winter, the Madden–Julian oscillation (MJO) is dominated by the equatorially trapped eastward-propagating mode (Madden and Julian 1972), whereas the boreal summer ISO exhibits eastward and northward propagations in the Indian Ocean (Yasunari 1979; Sikka and Gadgil 1980; Krishnamurti and Subrahmanyam 1982) and north-northwestward propagation over the western North Pacific (WNP) (Murakami et al. 1984; Wang and Xie 1997; Kemball-Cook and Wang 2001). There is a prominent seesaw oscillation between the equatorial Indian Ocean and the WNP (Zhu and Wang 1993). Most boreal summer ISO ends up in the WNP (Wang et al. 2006). Unfortunately, current general circulation models (GCMs) face difficulties in simulating the boreal summer ISO (Kim et al. 2008).

From late boreal summer to early fall (July–October), the global outgoing longwave radiation (OLR) exhibits the strongest ISO over the WNP, centered at the South China Sea and Philippine Sea (Fig. 1a). The equatorial Indian Ocean and Bay of Bengal have the secondary ISO centers, especially in the midsummer. Wang et al. (2005) hypothesized and Liu and Wang (2012) showed with a theoretical model that the atmosphere–ocean interaction, in cooperation with the instability caused by the local Hadley circulation and frictional boundary layer moisture convergence, can produce a self-sustained ISO over the Indian Ocean.

Over the WNP, the ISO mainly prevails during late boreal summer (Fig. 1b), when the WNP seasonal mean monsoon trough is strong and the corresponding cyclonic

* School of Ocean and Earth Science and Technology Contribution Number 9012 and International Pacific Research Center Publication Number 1017.

Corresponding author address: Dr. Bin Wang, IPRC, and Department of Meteorology, University of Hawai'i at Mānoa, 401 POST Bldg., 1680 East-West Road, Honolulu, HI 96822.
E-mail: wangbin@hawaii.edu

DOI: 10.1175/JCLI-D-12-00797.1

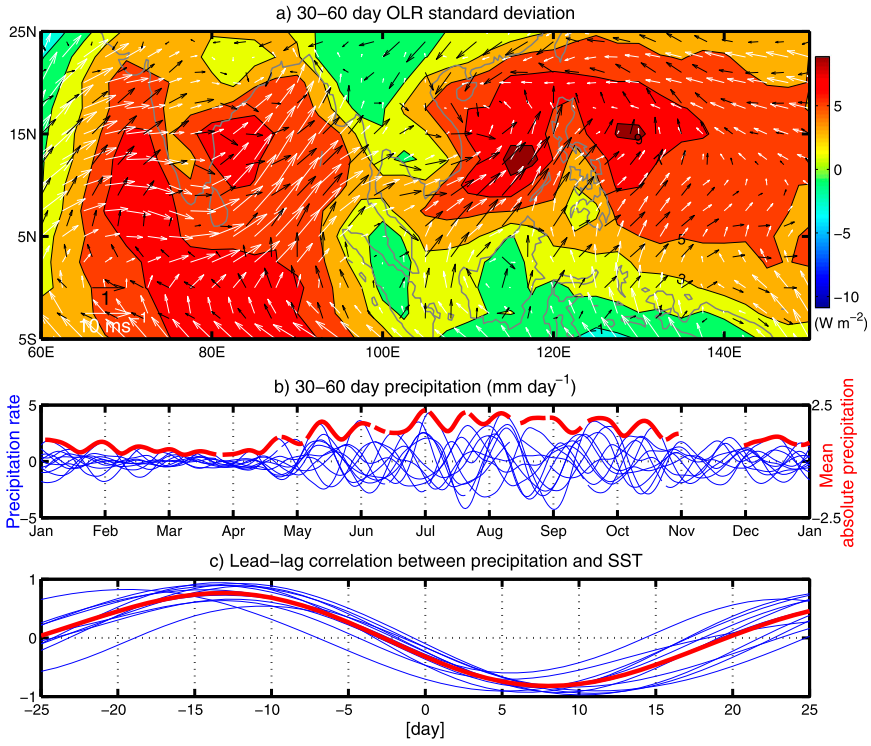

FIG. 1. Observed ISO over the WNP: (a) Climatological mean (1979–2010) surface (1000 hPa) winds (white vectors), variance of 30–60-day anomalous outgoing longwave radiation (OLR, shading), and the surface winds (black vector) that are correlated with the 30–60-day OLR minimum over the WNP (5°–20°N, 110°–140°E) during late boreal summer and early fall (July–October). The ISO wind vector represents the correlation coefficients of zonal and meridional components. The background mean variance (32-yr tropical, 40°S–40°N) has been removed. (b) Time series of 30–60-day anomalous daily rainfall rates for 1998–2009 (blue) and their 11-yr mean absolute precipitation (red) averaged over the WNP. The missing precipitation is not plotted. (c) Lead–lag correlation between the 30–60-day anomalous precipitation and SST averaged over the WNP for each year from 1998 to 2009 (blue) and their 11-yr mean (red). Negative lag day means how long the positive SST leads the positive precipitation. The precipitation and SST data are derived from the Tropical Rainfall Measuring Missions (TRMM)'s Microwave Imager (TMI) data (Wentz and Schabel 2000). The OLR data are obtained from the National Oceanic and Atmospheric Administration (NOAA) interpolated OLR data (available online at http://www.esrl.noaa.gov/psd/), and the wind data are obtained from the National Centers for Environmental Prediction (NCEP) reanalysis (Kalnay et al. 1996).

winds prevail (Fig. 1a). The sea surface temperature (SST) also displays a noticeable ISO. The lead–lag relationship between the precipitation and SST (Fig. 1c) indicates that a warm SST leads the positive precipitation anomaly by about 13 days and a cold SST tails the maximum precipitation by 7 days. Over the warm pool region of the western Pacific, the observed out-of-phase relationship between the SST and deep convection on the intraseasonal time scale also suggests an interesting avenue of feedback to the MJO (Waliser 1996), where the reduction in surface shortwave radiation by high clouds is the dominant mechanism that limits the SST of ''hot spots,'' although the increase in surface latent heat flux also plays a significant role. The hydrological cycle associated with the MJO is observed to act in the mode of a self-regulating oscillator. The thermodynamic/radiative feedbacks establish a feedback that regulates, in unison, the SST and hydrological cycle over the warm pool (Stephens et al. 2004). A similar SST–precipitation relationship was also found before for the eastward propagating MJO (Zhang 1996; Sui et al. 1997; Wang and Xie 1998; Woolnough et al. 2000) and northward propagation over Bay of Bengal (Sengupta et al. 2001; Kemball-Cook and Wang 2001; Fu et al. 2003; Rajendran and Kitoh 2006). Over the WNP summer monsoon trough, the enhanced intraseasonal precipitation corresponds to an enhanced cyclonic circulation anomaly (Wang et al. 2009). In Fig. 1a, the surface (1000 hPa)

winds associated with the strong ISO are in phase with the mean cyclonic winds. Meanwhile, the solar radiation flux is also in phase with the latent heat flux. The negative (positive) downward solar radiation flux and latent heat flux anomalies associated with the wet (dry) phase of the ISO both correspond to a negative (positive) SST tendency (Wang and Zhang 2002). In other seasons, however, when the WNP summer monsoon trough disappears and the ISO is very weak, the wind–evaporation/entrainment feedback would tend to demolish the oscillation and maintain the Philippine Sea anticyclone in the winter (Wang et al. 2000). These observations suggest the mean-state modulation of the atmosphere–ocean interaction of the ISO.

The signal of the ISO over the Philippine Sea (10°–20°N, 110°–135°E) usually originates from the equatorial western Pacific (5°S–5°N, 125°–150°E) (Wang et al. 2009). The area-averaged 30–60-day OLR standard deviations over these two boxed regions are 7.6 and 2.8 $\mathrm{W\,m^{-2}}$, respectively. We may think that the variances over the Philippine Sea consist of two parts. One is propagation induced, which is supposed to be the same as that over the equatorial western Pacific. The other part comes from the local intensification effects. The difference between these two boxes reflects the ''local'' effects. In this way we may estimate the local effects, and the results show that they are large. Although other processes may contribute to the local effects, we assume that atmosphere–ocean interaction may be a major contributor.

Concerning the ISO over the WNP, Wang and Zhang (2002) presented a hypothesis that the atmosphere–ocean interaction is essentially important: The cloud–radiation–SST feedback is always negative, and the wind–evaporation feedback, while depending on the background circulation, is also negative in the presence of the WNP summer monsoon trough. Thus, during the well-developed WNP monsoon period, these two negative feedback processes together should favor an oscillation in the WNP region. In this work, we will test this hypothesis and explain why the WNP experiences the strongest ISO in the late boreal summer season by building a conceptual atmosphere–ocean interaction model.

2. The atmosphere–ocean coupled model for the WNP ISO

The framework is derived from the atmosphere–ocean coupled model used for studying the warm pool system (Wang and Xie 1998) and the Indian summer monsoon system (Liu and Wang 2012), which is constructed based on the observed atmosphere–ocean interaction features associated with the WNP ISO (Fig. 1c). 1) The fact that the warm SST systemically leads the positive precipitation anomalies indicates that the SST can affect the sea level pressure through various processes such as convective parameterization (Philander et al. 1984), evaporation (Zebiak 1986), longwave Newtonian relaxation (Davey and Gill 1987), or equivalent SST gradient effect (Lindzen and Nigam 1987; Neelin 1989). 2) The SST is also affected by the shortwave radiation and sea surface evaporation (Wang and Xie 1998; Fu et al. 2003). 3) To represent the role of the planetary boundary layer, we use the Lindzen–Nigam model (Lindzen and Nigam 1987; Neelin 1989; Wang and Li 1993):

$$E\mathbf{V}_B + y\beta\mathbf{k}\times\mathbf{V}_B = -\nabla\phi_b + G\nabla T, \tag{1}$$

where y is the meridional displacement, $\mathbf{k}$ the vertical unit vector, $\mathbf{V}_B$ the boundary layer horizontal winds, ϕ_b the geopotential in the barotropic boundary layer that equals to the geopotential ϕ at the lower troposphere, T the SST, E the boundary layer friction, β the meridional variation of Coriolis parameter, and G the forcing parameter associated with the SST gradient. The Ekman pumping at the top of the boundary layer is

$$w = (d_1\partial_{xx} + d_1\partial_{yy} + d_2\partial_x + d_3\partial_y)\tilde{\phi}, \tag{2}$$

where x is the zonal displacement, $\tilde{\phi} = \phi - GT$, and boundary layer coefficients $\{d_1, d_2, d_3\} = \{E/(E^2+\beta^2y^2), -\beta(E^2-\beta^2y^2)/(E^2+\beta^2y^2)^2, -2E\beta^2y/(E^2+\beta^2y^2)^2\}$.

When wind anomalies are assumed to be adjusted to the geopotential anomaly on a time scale of $O(\varepsilon^{-1})$, the atmosphere–ocean interaction model can be written in pressure coordinates and on the β plane:

$$\varepsilon u - \beta y v = -\phi_x, \quad \beta y u = -\phi_y,$$

$$\phi_t + \mu\phi + C_0^2(u_x + v_y) = -\frac{R\Delta p}{2p_2C_p}Q - \frac{Rg}{2p_2C_p}\eta_T T,$$

$$T_t + \mu_o T = -\frac{0.622(1-A)S_0}{\rho_0 C_w h}\gamma Q - \frac{E_V}{\rho_0 C_w h}, \quad \text{and}$$

$$Q = -L_C q_L(u_x + v_y) + L_C\frac{\Delta p_B}{\Delta p}(q_B - q_L)w. \tag{3}$$

The perturbation evaporation is

$$E_V = r_v b_s \rho_a C_E L_C K_q(\overline{T} - 293.2)|V| + b_e\rho_a C_E L_C K_q|\overline{V}|T. \tag{4}$$

Equations (3) and (4) are a simplified version of that used in Wang and Xie (1998). For details the readers are

TABLE 1. Parameter values used in the box model.

$C_0 = 50\,\mathrm{m\,s^{-1}}$	Gravest gravity wave speed
$A = 0.06$	Sea surface albedo
$S_0 = 320\,\mathrm{W\,m^{-2}}$	Surface downward solar radiation flux under clear sky
$G = 49\,\mathrm{m^2\,s^{-2}\,K^{-1}}$	Coefficient of SST gradient forcing
$\Delta p, \Delta p_B = 400, 100\,\mathrm{hPa}$	Pressure depths of lower troposphere and boundary layer
$p_2 = 500\,\mathrm{hPa}$	Middle-tropospheric pressure
$\varepsilon, \mu = 3\,\mathrm{day^{-1}}$	Lower-tropospheric momentum and Newtonian damping
$E = 0.4\,\mathrm{day^{-1}}$	Boundary layer friction
$\mu_0 = 30\,\mathrm{day^{-1}}$	Oceanic mixed layer Newtonian damping
$q_B, q_L = 0.015, 0.008\,\mathrm{g\,Kg^{-1}}$	Mean specific humidity of boundary layer and lower troposphere for an SST of 28.5°C
$h = 20\,\mathrm{m}$	Oceanic mixed layer depth
$\overline{T} = 303\,\mathrm{K}$	Mean SST
$\lvert\overline{V}\rvert = 5\,\mathrm{m\,s^{-1}}$	Mean wind speed
$\eta_T = 33\,\mathrm{kg\,s^{-3}\,K^{-3}}$	SST forcing coefficient
$b_s, b_e = 0.4$	Coupling coefficients of shortwave radiation and evaporation feedbacks

referred to that paper. In (3) and (4), u and v are the lower-tropospheric anomalous velocities, ϕ the geopotential, $\overline{T}$ the mean SST, $|V|$ the perturbation wind speed, $|\overline{V}|$ the mean wind speed, and Q the perturbation diabatic heating that is attributable to the moisture convergence of the low troposphere and frictional boundary layer, respectively. Also, η_T is the SST forcing coefficient that represents how strong the SST affects the atmosphere; b_s and b_e are the coupling coefficients that determine the coupling efficiency of the shortwave radiation and evaporation feedbacks, respectively; and r_v is the control parameter that determines the direction of the wind-induced evaporation. Furthermore, C_0 is the gravest gravity wave speed, ε and μ the lower-tropospheric momentum and Newtonian damping, respectively; μ_o the mixed layer Newtonian cooling; h the oceanic mixed-layer depth; A the surface albedo; and S_0 the downward solar radiation flux reaching sea surface under clear sky. The perturbation cloud cover is assumed to be proportional to the perturbation precipitation with a coefficient γ. Finally, p_2, Δp, and Δp_B are the middle-tropospheric pressure and the lower-tropospheric and boundary layer pressure depths, respectively; q_B and q_L stand for the mean specific humidity at the boundary layer (1000–900 hPa) and the lower troposphere (900–500 hPa) (Wang 1988). Thus, the background moisture is represented by the boundary layer specific humidity q_B and lower tropospheric specific humidity q_L; both, in our model, are simply determined by the underlying mean SST (Table 1), which is assumed constant in time. In the summer monsoon trough the background moisture is high due to its association with a warm SST, whereas in the wintertime the same region has low background moisture due to the decreasing SST. We did not consider the background convergence effect on the background moisture.

The constant coefficients include the specific gas constant $R = 287\,\mathrm{J\,kg^{-1}\,K^{-1}}$, the specific heat at constant pressure $C_p = 1004\,\mathrm{J\,kg^{-1}\,K^{-1}}$, the latent heat of condensation $L_C = 2.5 \times 10^6\,\mathrm{J\,kg^{-1}}$, the water density $\rho_0 = 1.0 \times 10^3\,\mathrm{kg\,m^{-3}}$, the water heat capacity $C_w = 4186\,\mathrm{J\,kg^{-1}\,K^{-1}}$, the gravitational acceleration $g = 9.8\,\mathrm{m\,s^{-2}}$, the boundary air density $\rho_a = 1.2\,\mathrm{kg\,m^{-3}}$, the moisture transfer coefficient $C_E = 1.5 \times 10^{-3}$, the coefficient $K_q = 8.9 \times 10^{-4}\,\mathrm{K^{-1}}$ (Wang and Li 1993), and the meridional variation of Coriolis parameter $\beta = 2.3 \times 10^{-11}\,\mathrm{m^{-1}\,s^{-1}}$.

In this simple model, the total SST forcing is assumed to have double the strength of the SST-induced evaporation (i.e., $\eta_T = 2\rho_a C_E L_C K_q |\overline{V}|$). Sensitivity tests show that different η_T will not change the following results qualitatively except that a stronger η_T contributes to a faster oscillation. Since the precipitation is simply $Q\Delta p/(L_C g)$ (Wang 1988), the typical value $\gamma = 45.4\,\mathrm{kg\,s\,J^{-1}}$ means that an anomalous precipitation of $1\,\mathrm{mm\,day^{-1}}$ may result in an increase in total cloudiness by one-fifth. Unless otherwise mentioned, other parameters are listed in Table 1. Sensitivity experiments of the coefficients associated with the air–sea coupling will be discussed later.

The choice of the parameters that are associated with the air–sea interaction is not necessarily specific to the WNP because such an interaction can occur elsewhere. What is specific to the WNP is the season-dependent SST and circulation field. The SST is high in late boreal summer but decreases in other seasons, which determines the environmental relative humidity for the ISO development or decay.

Over the WNP, the mean state has certainly large seasonal variation (Fig. 2), and the cyclonic (anticyclonic) wind dominates in the summer (winter), and at the same time the ISO is also enhanced (suppressed). The direction of the air–sea interaction is controlled by the mean state and affected by the seasonal cycle. This is consistent with the observations on the seasonal time scale (Wang et al. 2000). In the summertime, the ISO and monsoon trough

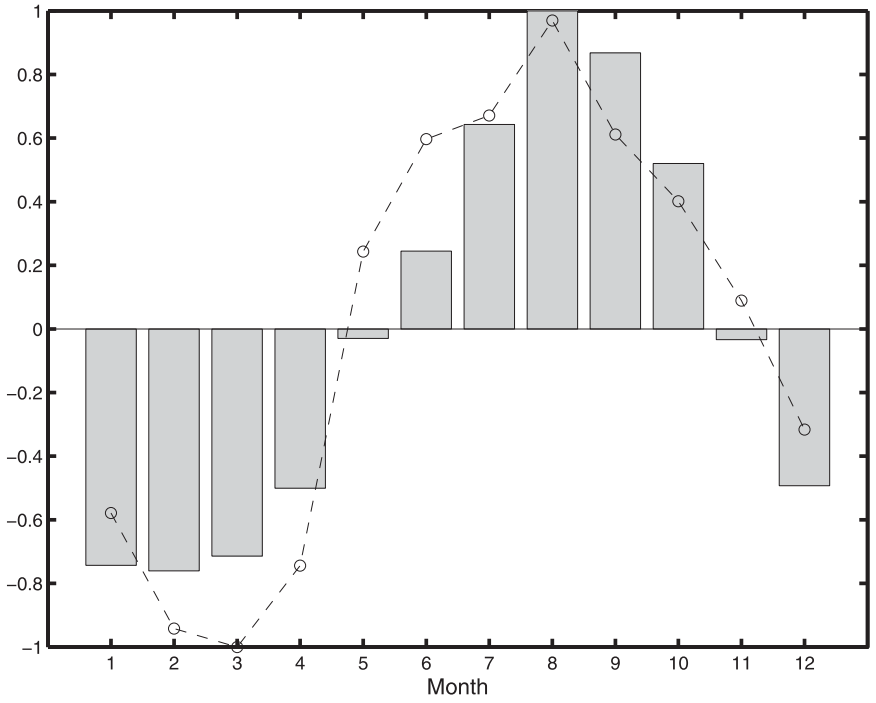

FIG. 2. Normalized climatological mean (1979–2010) annual anomalous western North Pacific monsoon index (WNPMI) (bars) (Wang and Fan 1999) and WNP (5°–20°N, 110°–140°E) ISO standard deviation (dot). The former is defined by the difference of 850-hPa area-averaged zonal winds between boxes (5°–15°N, 100°–130°E and 20°–30°N, 110°–140°E), which represents the cyclonic strength over the WNP. The latter is calculated from the 30–60-day filtered OLR. Magnitudes of the WNPMI and ISO are 8.3 m s^{-1} and 3.3 W m^{-2}, respectively.

have the same wind structure (Fig. 1a); thus, in the WNP monsoon trough, the latent heat flux is upward for a cyclonic anomaly and downward for an anticyclonic anomaly. We used one parameter r_v to represent the direction of the wind-induced evaporation anomaly: $r_v = 1$ is used for the upward evaporation associated with the cyclonic anomalies of the wet ISO, and $r_v = -1$ is used for the dry phase of the ISO. The evaporation magnitude is determined by the anomalous wind speed.

3. The one-box model

Substitution of first two equations of (3) into others yields linear governing equations of ϕ and T. To describe the local intensification effects over the WNP, we build a box model by assuming that ϕ and T have the specified structure of

$$\{\phi, T\} = \{\Phi, \Psi\} e^{-(x-x_0/x_L)^2-(y-y_0/y_L)^2}, \tag{5}$$

where Φ and Ψ are the amplitudes of the geopotential and SST anomalies, respectively, which are independent of x and y. The WNP oscillation center is located at $x_0 = 120°$E, $y_0 = 15°$N, and its horizontal scale is defined by $x_L = 20°$, $y_L = 10°$.

After substituting (5) into (3) we obtain the following linear system:

$$\partial_t(\Phi, \Psi)' = \mathbf{A}(x, y)(\Phi, \Psi)'. \tag{6}$$

Note that $\mathbf{A}(x, y)$ is the coefficient matrix defined from (3), thus the box model is averaged in the domain S:

$$\partial_t(\Phi, \Psi)' = \frac{\iint_S \mathbf{A}(x, y)\, dx\, dy}{\iint_S dx\, dy}(\Phi, \Psi)',$$

$$\text{where} \quad \{S: | e^{-(x-x_0/x_L)^2-(y-y_0/y_L)^2} > 0.01\}. \tag{7}$$

Equation (7) can be calculated from any initial conditions of Φ or Ψ. Sensitivity experiments show that the results are not sensitive to the size of the box domain S. For the atmosphere-only model, the SST anomaly is set to be zero.

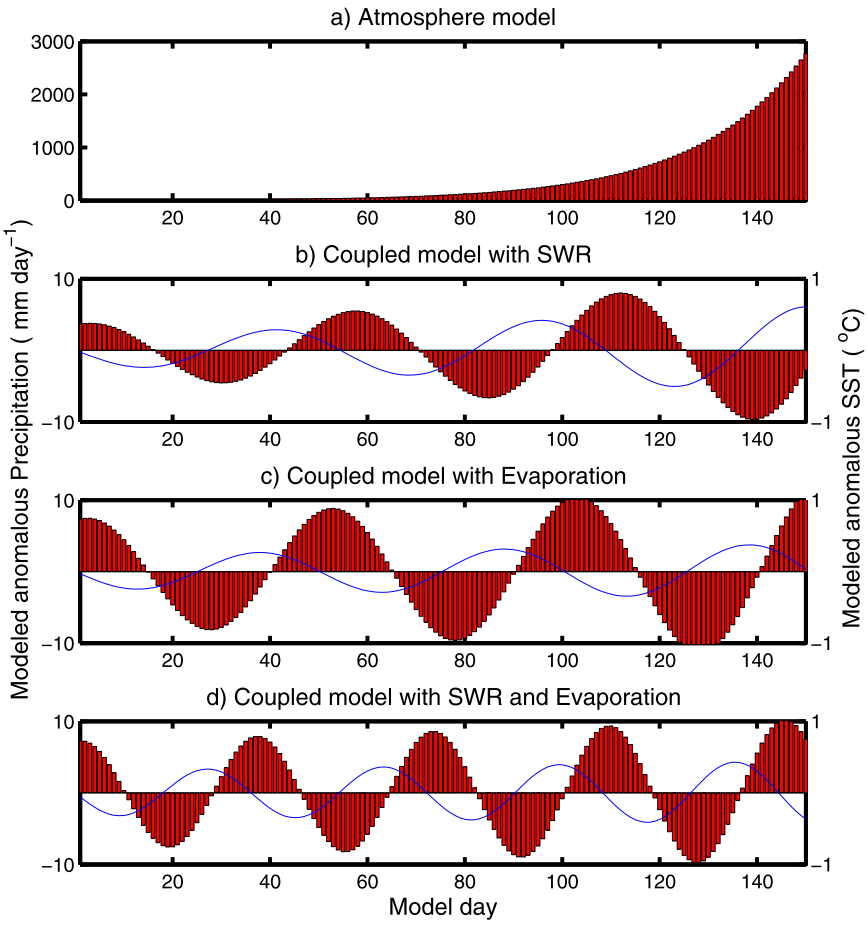

FIG. 3. Simulated precipitation rate (bars) and SST (lines) for (a) the atmosphere-only model, (b) the atmosphere–ocean coupled model with shortwave radiation (SWR) feedback, (c) the atmosphere–ocean coupled model with evaporation feedback, and (d) the atmosphere–ocean coupled model with both shortwave radiation and evaporation feedbacks.

4. A simulated stationary ISO over the WNP

Because of the instability caused by the frictional boundary layer (Xie and Wang 1996), this atmosphere-only model presents a developing mode with a growth rate of 0.04 day^{-1} (Fig. 3a). The instability is determined by the SST, and a warmer SST will enhance the instability. The atmosphere process alone only produces a monotonic mode, and no oscillation exists. However, inclusion of the atmosphere–ocean interaction will produce an oscillatory solution. The coupled model with either shortwave radiation (Fig. 3b) or evaporation feedback (Fig. 3c) alone produces a low-frequency oscillation with periods of 55 and 51 days, respectively. Meanwhile, a realistic phase relationship between the precipitation and SST is simulated: the warm SST leads the positive precipitation, and the positive precipitation tends to cool the sea surface through reducing the shortwave radiation and enhancing the sea surface evaporation.

This simulated oscillation can be explained by the negative feedbacks of the shortwave radiation and evaporation. In an active phase of the ISO, the strong precipitation and cloud cover will reduce the shortwave radiation and cool the sea surface (Fu et al. 2003). Meanwhile, both mean winds and ISO winds are cyclonic, and the resultant total winds tend to increase surface evaporation and also cool the sea surface. This cold SST will generate a lower-tropospheric high (Lindzen and Nigam 1987) as well as reduce the precipitation, which changes the wet phase to a dry phase of the ISO.

Atmospheric GCMs without air–sea coupling often simulate excessive intraseasonal variability over the WNP with maybe too much mean precipitation (Kim et al. 2011), while the propagation mechanism of the ISO, contributing to the simulated ISO in the atmospheric GCMs, is inhibited in our model. This simple model cannot simulate the ISO without the air–sea coupling.

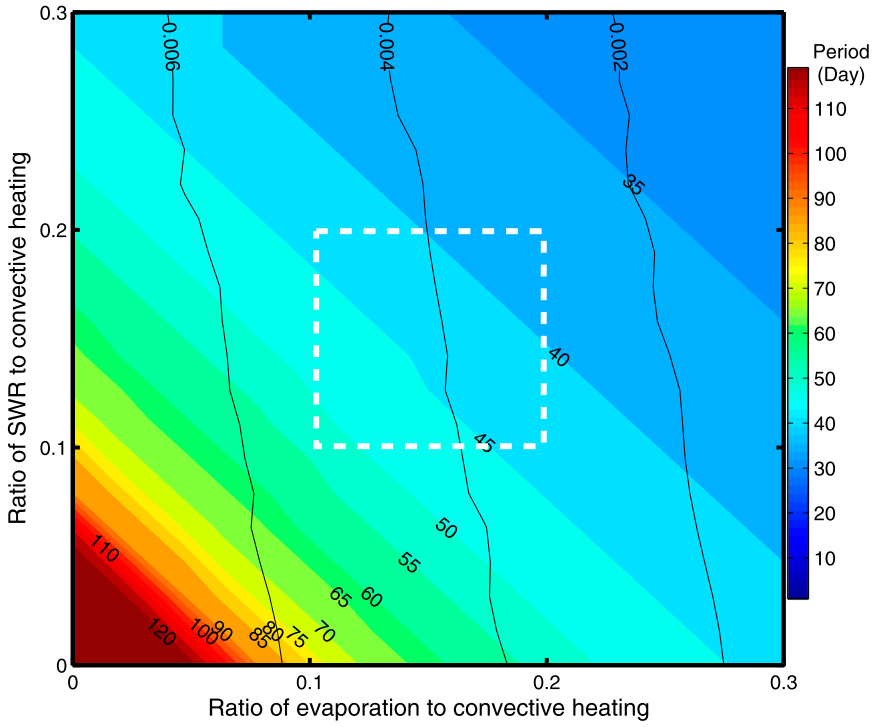

FIG. 4. Simulated period (shading) and growth rate (black contours, day^{-1}) as functions of the strength of evaporation and SWR. Shading for 120 days and longer are the same. White dashed rectangle denotes evaporation and SWR strength with their strength ratios of 0.1–0.2.

The combination of the shortwave radiation and evaporation feedbacks tends to reduce the oscillation's period compared to each individual feedback, producing an oscillation period of 36 days (Fig. 3d). Under current coupling coefficients $b_s = b_e = 0.4$, the ratios of the shortwave radiation and evaporation to the convective heating, which represent the strength of the air–sea coupling, are both 0.2. They are consistent with the observation of the ISO, which has a strength ratio of about 0.1–0.2 (Lin and Mapes 2004). Over a wide range of the air–sea coupling strength, the model always presents an oscillation on the intraseasonal scale (Fig. 4).

Since the shortwave radiation and evaporation present a negative feedback for the coupled system (Fig. 4), which tends to reverse one phase of the ISO to an opposite phase, the strong atmosphere–ocean interaction will accelerate this phase transition and reduce the oscillation's period (Bellon et al. 2008; Liu and Wang 2012). In this model, both the evaporation and shortwave radiative effects are negative, and the instability stems from the frictional boundary layer moisture convergence. The longwave radiative effect as formulated in Sobel and Gildor (2003) is not included. Because of the direct damping role of the SST-induced evaporation in (4), the evaporation is more efficient in damping the unstable mode than the shortwave radiation (Fig. 4).

The stationary oscillation can also be produced by other processes. For example, the stationary oscillation arising from the interaction among atmospheric radiation, cumulus convection, and surface moisture flux has been simulated in previous works (Hu and Randall 1994, 1995). In their works, only the SST-induced evaporation component in the evaporation feedback has been included, and it cannot represent the impact of the specific mean states on the evaporation anomalies. An oscillation of SST "hot spots" on time scales ranging from intraseasonal to subannual has been simulated by Sobel and Gildor (2003). In their work, a simple zero-dimensional atmospheric model was coupled to an oceanic mixed layer, and the temperature was assumed constant while the moisture was prognostic. The instability mechanism was cloud–radiative feedback, which led to effective gross moist instability. In this work, we focus on the wave dynamics by assuming constant background moisture, and the instability comes from the moisture convergence of frictional boundary layer. Furthermore, the wind-induced evaporation component was parameterized to be proportional to the precipitation by assuming that the ISO surface latent heat flux is in phase with the shortwave

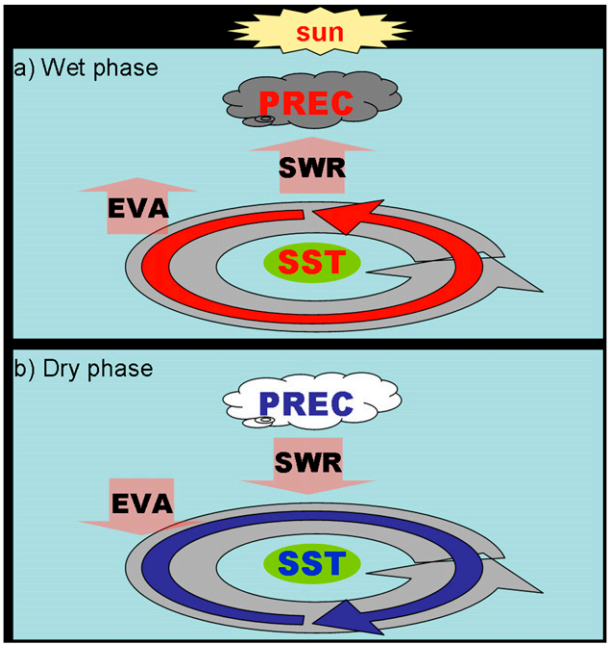

FIG. 5. Schematic diagram showing the atmosphere–ocean interaction mechanism of the ISO over the WNP summer monsoon trough region (gray cyclonic arrow) for (a) a wet phase of the ISO and (b) a dry phase of the ISO. Red (blue) symbols denote positive (negative) anomalies; upward (downward) arrows denote outgoing (incoming) shortwave radiation and evaporation at the sea surface. Other symbols are the same as those used in the text.

radiative energy flux in their work. Our results show that the specific mean circulation determines such a phase relationship. Different from the equatorial region where the shortwave radiation is more significant than the evaporation feedback (Waliser 1996), the same spatial structure between the perturbation and mean winds also provides an important evaporation feedback over the WNP, which is consistent with observations (Wang and Zhang 2002).

5. Concluding remarks

The self-sustained ISO simulated in this box model provides a plausible explanation as to why the strongest ISO prefers to occur over the WNP in late boreal summer. First, the strong WNP summer monsoon trough provides abundant moisture for the growth of the ISO, and the ISO disturbances can obtain instability from the frictional boundary layer moisture convergence (Wang 1988; Wang and Rui 1990b; Xie and Wang 1996; Maloney and Hartmann 1998). Second, the atmosphere–ocean interaction is the key for exciting the stationary ISO (Fig. 5). Associated with the cyclonic mean winds of the monsoon trough, the shortwave radiation and evaporation both suppress the growth of the SST and reverse a wet phase to a dry phase or vice versa.

In other seasons, the intraseasonal variability becomes damped without the WNP monsoon trough (Fig. 1b). The lack of the moisture source should be one of the reasons, but more importantly, the cyclonic mean winds over the WNP disappear or become anticyclonic during winter and spring. In the presence of boreal winter basic state, the surface evaporation associated with the anomalous winds would provide a positive feedback for the SST. For example, under the anticyclonic mean winds, $r_v = -1$ is selected for the wet phase of the ISO, while $r_v = 1$ for the dry phase of the ISO. As such, the model produces a monotonic developing mode (not shown), although the shortwave radiation still provides a negative feedback for the SST. This result supports the WNP subtropical high–warm ocean interaction theory for explanation of the ENSO prolonged impacts on the East Asian monsoon (Wang et al. 2000, 2013).

The cloud–radiation–SST feedback and the wind–evaporation feedback are two physical processes that are involved in atmosphere–ocean interaction over the warm pool ocean. They are not mechanisms per se. Wang and Xie (1998) have shown that these two processes are involved in the interaction between low-frequency equatorial waves and oceanic mixed layer (without mean flow). This interaction mechanism can change the wave propagation and produces instability. The mechanism proposed here, although involves the same two processes, is different from previous studies such as that of Wang and Xie (1998). It invokes the critical regulation of the seasonal varying mean flows on the interaction of the convectively coupled ISO anomaly and oceanic mixed layer. Our new mechanism points out that the nature of the air–sea feedback processes strictly depends on the mean state: for a summer monsoon trough (cyclonic circulation), this feedback is negative, which maintains and amplifies the ISO. On the other hand, for a winter mean basic state these feedback processes provide a positive feedback, thus damping the ISO and sustaining a Philippine Sea anticyclone. What is new in the present study is that we have theoretically illustrated this mechanism. This is the major purpose of the present study—that is, to address the question of why the WNP summer monsoon region tends to have the maximum ISO variance. The proposed processes can be generally applicable to other tropical monsoon trough regions such as Indian monsoon trough region and eastern Pacific monsoon trough region, while the WNP region has least interference with and is least affected by the configuration, so this mechanism may be most relevant to WNP region.

Over the WNP, many current models have notorious deficiency in simulating correct mean state that regulates the air–sea interaction, and some models cannot even represent the monsoon trough (e.g., Kang et al.

TABLE 2. Coupled atmosphere–ocean models used in the control experiments

No.	Institute	Model
1	Australian Bureau of Meteorology (BOM), Australia	BOM Research Centre (BMRC) Atmospheric Model, version 3 (BAM3), coupled with the Australian Community Ocean Model, version 2 (ACOM2)
2	Centro Euro-Mediterraneo sui Cambiamenti Climatici (CMCC), Italy	ECHAM5 coupled with Ocean Parallélisé, version 8.2 (OPA8.2)
3	Environment Canada (EC), Canada	Global Environment Multiscale (GEM) model
4	European Centre for Medium-Range Weather Forecasts (ECMWF), United Kingdom	Integrated Forecast System (IFS) coupled with the Hamburg Ocean Primitive Equation (HOPE) model
5	Japan Meteorological Agency (JMA), Japan	JMA atmosphere–ocean CGCM
6	National Centers for Environmental Prediction (NCEP), United States	Global Forecast System (GFS) coupled with the Modular Ocean Model, version 3 (MOM3)
7	Pusan National University (PNU), South Korea	NCEP GFS using a Relaxed Arakawa–Shubert (RAS) scheme coupled with MOM3
8	Seoul National University (SNU), South Korea	SNU AGCM coupled with MOM3
9	University of Hawaii (UH), Hawaii	Hybrid CGCM (UH-HCM)
10	University of Hamburg, Germany	Parallel Ocean Program, version 2.0.1 (POP)–Ocean Atmosphere Sea Ice Soil, version 3.0 (OASIS)–ECHAM Model, version 1 (POEM1)
11	University of Hamburg, Germany	POP–OASIS–ECHAM Model, version 2 (POEM2)

2002; Wang et al. 2004). We have analyzed the results from the control experiments performed by 11 coupled atmosphere–ocean models (see the list of models in Table 2) that participated in the intraseasonal variability hindcast experiment (Zhang et al. 2013) for a 20-yr period (1989–2008) simulation. The results show that the models with better mean state present a better ISO (20–100 day) simulation over the WNP (Fig. 6), which indicates that an accurate simulation of the WNP mean state is a prerequisite for a good ISO simulation. Thus, the deficiencies

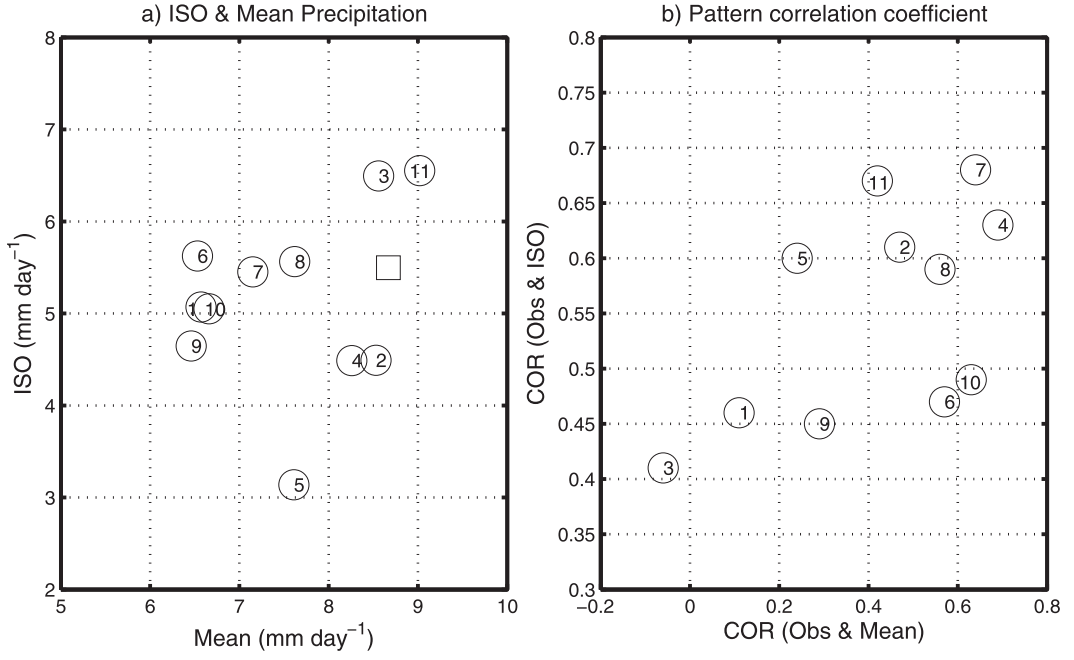

FIG. 6. (a) Relationship between the 20-yr (1989–2008) mean ISO precipitation standard deviations and 20-yr mean seasonal mean precipitation averaged over the WNP (5°–20°N, 110°–140°E) during July–October. The circles denote results simulated by 11 coupled GCMs and the square denotes that derived from observations (NCEP reanalysis). The models with stronger mean precipitation tend to have stronger ISO variability. (b) Pattern correlation coefficients between the observation and model simulations for the July–October ISO precipitation standard deviation (ordinate) and seasonal mean precipitation (abscissa) averaged over the WNP during the 20 years. The models with a more realistic simulation of the mean WNP precipitation also tend to simulate more realistic ISO variability.

in mean state simulation will have a direct consequence on the models' performance in simulation of the ISO. The present study may also have important implications as to how to improve numerical modeling of the ISO.

In this work, we neglected the nonlinear processes in the WNP ISO. For example, the vertical shear of mean winds, which is important for the growth of Rossby waves (Xie and Wang 1996), will be rectified by the ISO. Meanwhile, the high-frequency quasi-biweekly mode, which prevails in the warm pool (Murakami and Frydrych 1974; Chen and Chen 1995; Chatterjee and Goswami 2004; Kikuchi and Wang 2009), also provides an important scale interaction for the ISO. These processes should be addressed in the future.

Acknowledgments. The authors thank Dr. June-Yi Lee for providing the model data from the intraseasonal variability hindcast experiment. This study has been supported by Climate Dynamics Program of the National Science Foundation under Award AGS-1005599, the NOAA/MAPP project Award NA10OAR4310247, AMDT1, and the APEC climate center. The authors also acknowledge support from International Pacific Research Center (IPRC), which is partially supported by the Japan Agency for Marine-Earth Science and Technology (JAMSTEC) through their sponsorship of research activities at the IPRC.

REFERENCES

Bellon, G., A. H. Sobel, and J. Vialard, 2008: Ocean–atmosphere coupling in the monsoon intraseasonal oscillation: A simple model study. *J. Climate,* **21,** 5254–5270.

Chatterjee, P., and B. N. Goswami, 2004: Structure, genesis and scale selection of the tropical quasi-biweekly mode. *Quart. J. Roy. Meteor. Soc.,* **130,** 1171–1194.

Chen, T.-C., and J.-M. Chen, 1995: An observational study of the South China Sea monsoon during the 1979 summer: Onset and life cycle. *Mon. Wea. Rev.,* **123,** 2295–2318.

Davey, M. K., and A. E. Gill, 1987: Experiments on tropical circulation with a simple moist model. *Quart. J. Roy. Meteor. Soc.,* **113,** 1237–1269.

Fu, X., B. Wang, T. Li, and J. P. McCreary, 2003: Coupling between northward-propagating, intraseasonal oscillations and sea surface temperature in the Indian Ocean. *J. Atmos. Sci.,* **60,** 1733–1753.

Hu, Q., and D. A. Randall, 1994: Low-frequency oscillations in radiative–convective systems. *J. Atmos. Sci.,* **51,** 1089–1099.

——, and ——, 1995: Low-frequency oscillations in radiative–convective systems. Part II: An idealized model. *J. Atmos. Sci.,* **52,** 478–490.

Kalnay, E., and Coauthors, 1996: The NCEP/NCAR 40-Year Reanalysis Project. *Bull. Amer. Meteor. Soc.,* **77,** 437–471.

Kang, I.-S., and Coauthors, 2002: Intercomparison of the climatological variations of Asian summer monsoon precipitation simulated by 10 GCMs. *Climate Dyn.,* **19,** 383–395.

Kemball-Cook, S., and B. Wang, 2001: Equatorial waves and air–sea interaction in the boreal summer intraseasonal oscillation. *J. Climate,* **14,** 2923–2942.

Kikuchi, K., and B. Wang, 2009: Global perspective of the quasi-biweekly oscillation. *J. Climate,* **22,** 1340–1359.

Kim, D., A. H. Sobel, D. M. W. Frierson, E. D. Maloney, and I.-S. Kang, 2011: A systematic relationship between intraseasonal variability and mean state bias in AGCM simulations. *J. Climate,* **24,** 5506–5520.

Kim, H.-M., I.-S. Kang, B. Wang, and J.-Y. Lee, 2008: Interannual variations of the boreal summer intraseasonal variability predicted by ten atmosphere–ocean coupled models. *Climate Dyn.,* **30,** 485–496.

Krishnamurti, T. N., and D. Subrahmanyam, 1982: The 30–50 day mode at 850 mb during MONEX. *J. Atmos. Sci.,* **39,** 2088–2095.

Lin, J.-L., and B. E. Mapes, 2004: Radiation budget of the tropical intraseasonal oscillation. *J. Atmos. Sci.,* **61,** 2050–2062.

Lindzen, R. S., and S. Nigam, 1987: On the role of the sea surface temperature gradients in forcing low-level winds and convergence in the tropics. *J. Atmos. Sci.,* **44,** 2418–2436.

Liu, F., and B. Wang, 2012: A conceptual model for self-sustained active-break Indian summer monsoon. *Geophys. Res. Lett.,* **39,** L20814, doi:10.1029/2012GL053663.

Madden, R. A., 1986: Seasonal variations of the 40–50 day oscillation in the tropics. *J. Atmos. Sci.,* **43,** 3138–3158.

——, and P. R. Julian, 1972: Description of global-scale circulation cells in the tropics with 40–50 day period. *J. Atmos. Sci.,* **29,** 1109–1123.

Maloney, E. D., and D. L. Hartmann, 1998: Frictional moisture convergence in a composite life cycle of the Madden–Julian oscillation. *J. Climate,* **11,** 2387–2403.

Murakami, T., and M. Frydrych, 1974: On the preferred period of upper wind fluctuations during the summer monsoon. *J. Atmos. Sci.,* **31,** 1549–1555.

——, T. Nakazawa, and J. He, 1984: On the 40–50 day oscillations during the 1979 Northern Hemisphere summer I: Phase propagation. *J. Meteor. Soc. Japan,* **62,** 440–468.

Neelin, J. D., 1989: On the interpretation of the Gill model. *J. Atmos. Sci.,* **46,** 2466–2468.

Philander, S. G. H., T. Yamagata, and R. C. Pacanowski, 1984: Unstable air–sea interactions in the tropics. *J. Atmos. Sci.,* **41,** 604–613.

Rajendran, K., and A. Kitoh, 2006: Modulation of tropical intraseasonal oscillations by ocean–atmosphere coupling. *J. Climate,* **19,** 366–391.

Sengupta, D., B. N. Goswami, and R. Senan, 2001: Coherent intraseasonal oscillations of ocean and atmosphere during the Asian summer monsoon. *Geophys. Res. Lett.,* **28,** 4127–4130.

Sikka, D. R., and S. Gadgil, 1980: On the maximum cloud zone and the ITCZ over Indian longitudes during the southwest monsoon. *Mon. Wea. Rev.,* **108,** 1840–1853.

Sobel, A. H., and H. Gildor, 2003: A simple time-dependent model of SST hot spots. *J. Climate,* **16,** 3978–3992.

Stephens, G. L., P. J. Webster, R. H. Johnson, R. Engelen, and T. L'Ecuyer, 2004: Observational evidence for the mutual regulation of the tropical hydrological cycle and tropical sea surface temperatures. *J. Climate,* **17,** 2213–2224.

Sui, C.-H., X. Li, K.-M. Lau, and D. Adamac, 1997: Multiscale air–sea interactions during TOGA COARE. *Mon. Wea. Rev.,* **125,** 448–462.

Waliser, D. E., 1996: Formation and limiting mechanisms for very high sea surface temperature: Linking the dynamics and the thermodynamics. *J. Climate,* **9,** 161–188.

Wang, B., 1988: Dynamics of tropical low-frequency waves: An analysis of the moist Kelvin wave. *J. Atmos. Sci.,* **45,** 2051–2065.

——, and H. Rui, 1990a: Synoptic climatology of transient tropical intraseasonal convection anomalies. *Meteor. Atmos. Phys.,* **44,** 43–61.

——, and ——, 1990b: Dynamics of coupled moist Kelvin–Rossby waves on an equatorial beta-plane. *J. Atmos. Sci.,* **47,** 397–413.

——, and T. Li, 1993: A simple tropical atmospheric model of relevance to short-term climate variation. *J. Atmos. Sci.,* **50,** 260–284.

——, and X. Xie, 1997: A model for the boreal summer intraseasonal oscillation. *J. Atmos. Sci.,* **54,** 72–86.

——, and ——, 1998: Coupled modes of the warm pool climate system. Part I: The role of air–sea interaction in maintaining the Madden–Julian oscillation. *J. Climate,* **11,** 2116–2135.

——, and Z. Fan, 1999: Choice of South Asian summer monsoon indices. *Bull. Amer. Meteor. Soc.,* **80,** 629–638.

——, and Q. Zhang, 2002: Pacific–East Asian teleconnection. Part II: How the Philippine Sea anticyclone is established during El Niño development. *J. Climate,* **15,** 3252–3265.

——, R. Wu, and X. Fu, 2000: Pacific–East Asia teleconnection: How does ENSO affect East Asian climate? *J. Climate,* **13,** 1517–1536.

——, I.-S. Kang, and J.-Y. Lee, 2004: Ensemble simulations of Asian–Australian monsoon variability by 11 AGCMs. *J. Climate,* **17,** 803–818.

——, P. J. Webster, and H. Teng, 2005: Antecedents and self-induction of the active-break South Asian monsoon unraveled by satellites. *Geophys. Res. Lett.,* **32,** L04704, doi:10.1029/2004GL020996.

——, ——, K. Kikuchi, T. Yasunari, and Y. Qi, 2006: Boreal summer quasi-monthly oscillation in the global tropics. *Climate Dyn.,* **27,** 661–675.

——, F. Huang, Z. Wu, J. Yang, X. Fu, and K. Kikuchi, 2009: Multi-scale climate variability of the South China Sea monsoon: A review. *Dyn. Atmos. Oceans,* **47,** 15–37.

——, B. Q. Xian, and J. Y. Lee, 2013: Subtropical high predictability establishes a promising way for monsoon and tropical storm predictions. *Proc. Natl. Acad. Sci. USA,* **110,** 2718–2722, doi:10.1073/pnas.1214626110.

Wentz, F. J., and M. Schabel, 2000: Precise climate monitoring using complementary satellite data sets. *Nature,* **403,** 414–416.

Woolnough, S. J., J. M. Slingo, and B. J. Hoskins, 2000: The relationship between convection and sea surface temperature on intraseasonal timescales. *J. Climate,* **13,** 2086–2104.

Xie, X., and B. Wang, 1996: Low-frequency equatorial waves in vertically sheared zonal flows. Part II: Unstable waves. *J. Atmos. Sci.,* **53,** 3589–3605.

Yasunari, T., 1979: Cloudiness fluctuations associated with the Northern Hemisphere summer monsoon. *J. Meteor. Soc. Japan,* **57,** 227–242.

Zebiak, S. E., 1986: Atmospheric convergence feedback in a simple model for El Niño. *Mon. Wea. Rev.,* **114,** 1263–1271.

Zhang, C., 1996: Atmospheric intraseasonal variability at the surface in the tropical western Pacific Ocean. *J. Atmos. Sci.,* **53,** 739–758.

——, J. Gottschalck, E. D. Maloney, M. W. Moncrieff, F. Vitart, D. E. Waliser, B. Wang, and M. C. Wheeler, 2013: Cracking the MJO nut. *Geophys. Res. Lett.,* **40,** 1223–1230, doi:10.1002/grl.50244.

Zhu, B., and B. Wang, 1993: The 30–60 day convection seesaw between the tropical Indian and western Pacific Oceans. *J. Atmos. Sci.,* **50,** 184–199.